ORIENTATION-INDEPENDENT BUBBLE TRAP WITH INTERNAL PARTITION FOR ROBUST OPERATION OF MICROFLUIDIC SYSTEMS

Bhavagyna Vegunta, Charmaine Lui, Max Kim, Joshua Tran, Maya Papez,
Anand K. Ramasubramanian, Sang-Joon John Lee*

San Jose State University, San Jose, California, USA
*Corresponding authors: sang-joon.lee@sjsu.edu

SUPPLEMENTARY INFORMATION

Video Files

The following video clips provide functional demonstrations of the bubble trap under different conditions as noted. The demonstration fluid is deionized water with red food coloring. Except for the manual syringe demonstration, flow was drawn from an open supply reservoir through a bubble trap by a programmable syringe pump (Harvard Apparatus 11 Plus). When using the syringe pump, air was introduced with small (~10 µL) and large (~50 µL) doses by manually lifting the otherwise submerged tubing inlet from the upstream reservoir.

MOVIE S1: movie_s1_manual_syringe.mp4
Air slug removal with manual syringe

MOVIE S2: movie_s2_low_flow_rate.mp4
Bubble removal at 1.2 mL/min flow rate

MOVIE S3: movie_s3_high_flow_rate.mp4
Bubble removal at 6.0 mL/min flow rate

MOVIE S4: movie_s4_360_degree_rotation.mp4
Bubble removal while rotating 360°

Calculation and Experimental Measurement of Limiting Volume

The total internal volume inside a spherical cavity is:

$$V_{internal} = 4\pi r^3/3$$

where r is the internal radius. The internal height of remaining liquid with respect to the equatorial plane is represented by h_{liquid}. Bubble trap operating conditions necessitate that h_{liquid} be greater than the internal depth of the egress port, h_{egress} (Fig. S1).

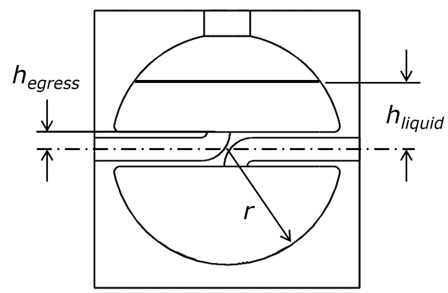

Fig. S1. Geometric layout for calculation of time to limiting capacity.

To find the maximum volume of internally accumulated gas (i.e., the limiting capacity), we can use the geometry of the section of the sphere cut by a plane at height h_{egress}. The volume of a hemisphere with radius r is $\frac{2}{3} \pi r^3$. The volume of a disk with the same radius r and height h_{egress} is $\pi r^2 h_{egress}$. By subtracting the volume of the disk from the volume of the hemisphere, we obtain the volume of gas above the plane at height h_{egress}. Therefore, the maximum volume of internally accumulated gas (i.e. limiting capacity) for bubble trap operating conditions can be defined as:

$$(V_{gas})_{max} = (\tfrac{2}{3} \pi r^3) - (\pi r^2 h_{egress})$$

For estimating the maximum volume of air which the bubble trap can accumulate before inability to remove bubbles, a closed system was assembled (Fig. 2). The micropump was initially set to a voltage at which the thermal flow sensor measures the flow to be 1 mL/min. Bubbles were then introduced by temporarily lifting upstream tubing above the liquid surface in the open reservoir for prescribed time intervals of ~2 s. The time to failure was the sum of time intervals during which air was deliberately introduced. Failure was recognized by an acute peak detected by the flow sensor located after the bubble trap, corresponding to the air accumulation capacity. The time of reaching this maximum limit was recorded for four replicate trials to quantify repeatability. The test was executed for a range of flow rates from 1 mL/min to 6 mL/min at 1 mL/min intervals. The bubble trap was filled to approximately 75% fill height and the system was run for 1 minute. During the experimental performance testing, the approximate volume of each bubble fluctuated depending on flow rate and ranged from 0.2 mL at 6 mL/min flow rate to 0.03 mL at 1 mL/min flow rate, computed from the nominal pumping flow rate times a relatively consistent air exposure interval.

Fig. S2A shows the time required to reach the maximum allowable air volume (i.e., the limiting capacity) inside the bubble trap as a function of flow rate. The plot shows good repeatability over four experimental trials, with standard deviation of less than 0.1 minute at any given flow rate. The experimental data are consistent with a theoretically calculated curve for the time of filling (superimposed), assuming a 100% volume fraction of gas that is continuously separated from the incoming fluid. The air volume at failure (i.e., exceeding the maximum allowable capacity) has no correlation with flow rate (Pearson correlation coefficient of 0.21 across the 24 measurements) (Fig. S2B). The limiting capacity is independent of flow rate, demonstrating a wide operating range.

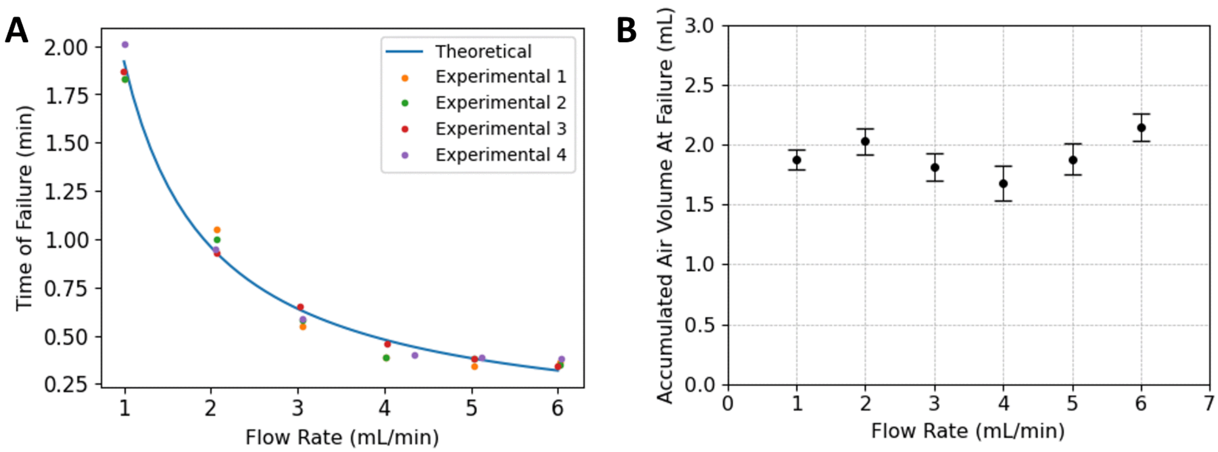

Fig. S2 Time to reach limiting capacity vs. flow rate (A). Internally accumulated internal air volume at failure vs. flow rate (B). Plots show mean with standard deviation error bars.

Replicate Runs of Long-Duration Testing

Figure S3 shows replicate runs of long-duration experiments (with a representative case shown in Section 3). Fig. S3A shows a case with a higher rate of bubble occurrence than Fig. 4, and Fig. S3C shows a more severe case with a suspected breach in the system. The bubble traps were operated continuously with deionized water at 37 °C for 24 h. The plots show flow rate vs. time, for which the prescribed flow rate was nominally ~5 mL/min in each case. The flow readings in Figs. S3A and S3C are plotted as a moving average of 10 consecutive data points to account for the high-frequency (100 Hz) driving oscillation of the micropump. Before the bubble trap, air bubbles appear as acute spikes, and occur randomly over the 24 h tests. The swarm plots data points in Figs. S3B and S3D correspond to instances of flow rate spikes greater than or equal to 15 mL/min.

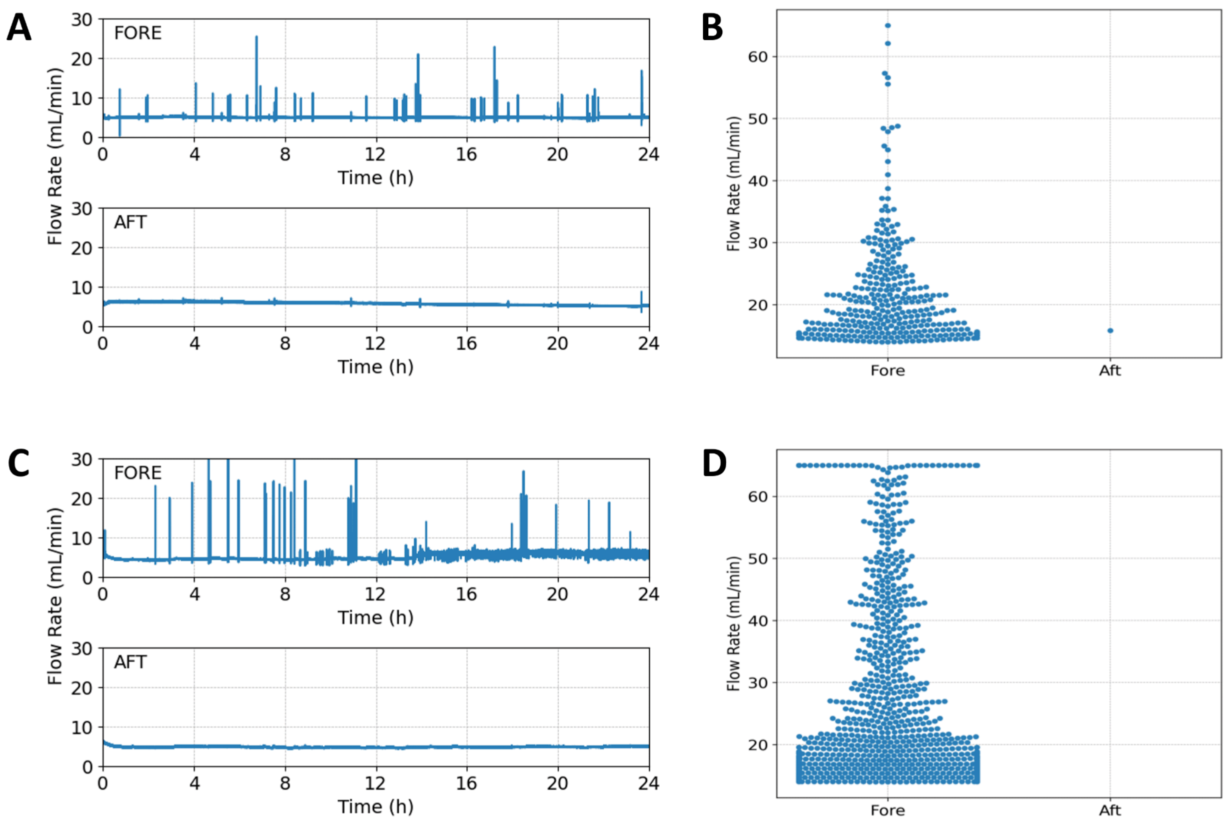

Fig. S3 Supplementary running average plots of long-duration testing, with more frequent bubbles (A, B), and an extreme case (C, D). In all cases, the bubble trap demonstrates ability to mitigate bubbles, evidenced in absence of spikes in S2A and S2C and the dramatic decrease in flow rate spikes in the AFT measurements.

Orientation Analysis of Endothelial Cells

Figure S4 illustrates the identification of nuclei for orientation analysis using the OrientationJ plugin for ImageJ [https://bigwww.epfl.ch/demo/orientation/] from a representative binarized image of endothelial cells. For analysis of any given condition (e.g., static vs. flow, normal vs. microgravity), approximately 160 nuclei were randomly sampled from images that were captured from two separate channels (between 61 and 88 nuclei per image).

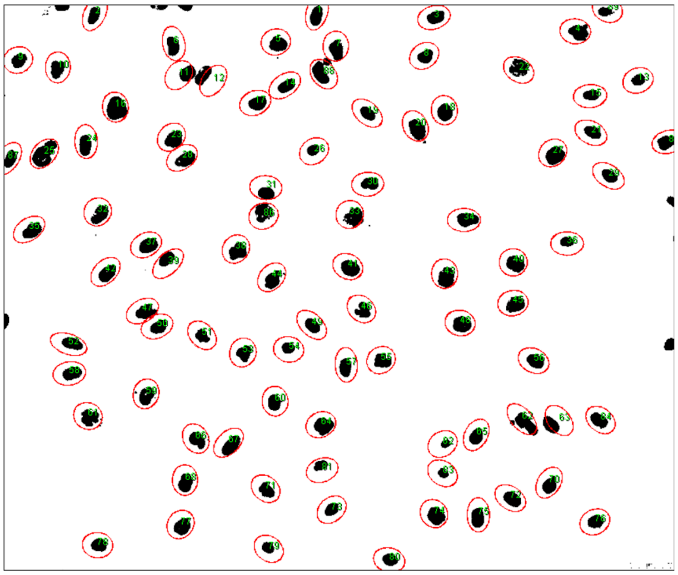

Fig. S4 Representative feature identification and image analysis for orientation of nuclei using OrientationJ. The field of view is approximately 850 µm × 720 µm.